Solid State Ionics 344 (2020) 115091

Contents lists available at ScienceDirect

Solid State Ionics

journal homepage: www.elsevier.com/locate/ssi

Comparison of in-situ Raman studies of SOFC with thick single-crystal and thin-film magnetron sputtered membranes

D.A. Agarkov[a,b,*], I.N. Burmistrov[a,b], G.M. Eliseeva[a], I.V. Ionov[c], S.V. Rabotkin[c], V.A. Semenov[c], A.A. Solovyev[c], I.I. Tartakovskii[a,d], S.I. Bredikhin[a,b]

[a] Institute of Solid State Physics RAS, 2 Academician Osipyan Str., 142432 Chernogolovka, Moscow Distr., Russia
[b] Moscow Institute of Physics and Technology, Institutsky lane 9, 141700 Dolgoprudny, Moscow District, Russia
[c] Institute of High Current Electronics SB RAS, Akademicheskiy pr., 2/3, 634055 Tomsk, Russia
[d] National Research University Higher School of Economics, Myasnitskaya. 20, 101000 Moscow, Russia

ARTICLE INFO

Keywords:
Solid oxide fuel cells
Electrolyte-supported
Single-crystal solid electrolyte
Anode-supported
Thin-film electrolyte
Overpotential

ABSTRACT

In current work, we conducted comparative studies of electrolyte-supported and anode-supported solid oxide fuel cells by means of electrochemical techniques (studies of I-V curves and impedance spectroscopy) as well as using Raman spectroscopy from the inner interface of the anode electrode and solid electrolyte. Electrolyte-supported (ESC) SOFCs were based on thick single-crystalline 8YSZ anion conductor membrane and had multilayered composite electrodes. Anode-supported cells (ASC) were based on thick two-layered commercially available anode supports, the thin-film electrolyte was deposited using a magnetron sputtering technique. Comparative studies showed a significant dependence of 460 cm^{-1} Raman peak both on fuel mixture composition and current load applied to the cell. Linear dependences of OCV on normalized peak area gave an opportunity to estimate local anodic overpotential on the current load applied for both SOFC structures. Application of ASC model cells gave an opportunity to significantly extend a range of current loads applied. Analysis of impedance spectra gave the opportunity to study the structure of complex resistance as well as the structure of local anodic overpotential obtained.

1. Introduction

Power plants based on solid oxide fuel cells (SOFC) technology are among the most promising generators of electricity and highly-potential heat [1,2] mainly because of their high efficiency for production of both electrical [3] and heat energy [4,5]. Another important advantage of solid oxide fuel cell is multifuel nature [6,7], SOFC can operate using chemical energy of oxidation of methane [8,9], propane [10,11], butane [12,13], dimethoxymethane [14], petroleum gas [15], dimethyl ether [16], ethanol [17], bioethanol [18], and even prepared diesel fuel [19,20]. Ecological friendliness [21,22], long lifetime [23] and service interval due to the absence of moving parts are also worth noticing when listing benefits of solid oxide fuel cell based power systems.

Electrolyte-supported solid oxide fuel cells (ESC) are one of the most advanced SOFC types [24] due to a relatively simple fabricating route which consists of cheap and scalable operations, which were optimized in other fields (e.g. microelectronics industry). Application of electrolyte support leads to relatively high working temperatures (800–900 °C). Elevated working temperature of ESC SOFC causes special requirements to materials, rapid degradation of the components and limited lifetime. Lowering of working temperature is strictly limited by dramatic increase of electrolyte membrane ionic resistance. One needs to use thin-film solid electrolyte in order to reduce its role in full resistance and in order to lower the operating temperature of the SOFC based system. There are different approaches to reach this goal, they can be divided into groups in accordance to support element used instead of solid electrolyte membrane: anode-supported cells (ASC) [25,26], cathode-supported cells (CSC) [27,28], cells with metal support (MSC) [29,30], and cells with inert support (ISC) [31,32].

In the case of ASC, CSC, MSC, and ISC approach there is a thin-film electrolyte, its role in total resistance is much lower than in the case of ESC SOFCs. This means that the role of electrodes is higher, one needs to study them carefully in order to optimize their composition and microstructure and minimize the resistance of the cell. Determination of fuel oxidation mechanism on the anode electrode is rather important for its optimization. Traditional electrochemical techniques (e.g. measurement of I-V curves, impedance spectroscopy, chronopotentiometry, etc.) are rather cumulative and give no information about electrode

* Corresponding author at: Institute of Solid State Physics RAS, 2 Academician Osipyan Str., 142432 Chernogolovka, Moscow Distr., Russia.
E-mail address: agarkov@issp.ac.ru (D.A. Agarkov).

https://doi.org/10.1016/j.ssi.2019.115091
Received 21 July 2019; Received in revised form 29 August 2019; Accepted 9 October 2019

processes which happen during SOFC operation. Different ex-situ methods (e.g. structural or element analysis ones) can give more specific information, but do not give the opportunity to study an operating fuel cell. One of the promising in-situ techniques for this purpose is Raman spectroscopy, which is remote, molecular specific, non-invasive [33,34], more than 90 years of the history of its application gave an opportunity to collect a large base of spectra for different compounds, including all traditional SOFC materials. Nowadays Raman spectroscopy is widely used in a field of solid oxide fuel cells for material characterization [35,36], studies of carbon deposition [37,38], fuel oxidation [39,40] as well as sulfur tolerance [41,42] and mechanical stress distribution [43,44]. In-situ studies of SOFC by means of Raman spectroscopy [45–47] do not influence an operating fuel cell, but these researches are limited by outer boundaries of a model sample when electrochemical processes mainly happen in the vicinity of SOFC inner interfaces. Special geometry, which gives an opportunity to reach an inner interface between solid electrolyte and anode electrode was developed and tested in our research group previously [48–50], as well as combined technique for simultaneous studies by means of optical and electrochemical techniques [50–52]. In previous works, we conducted studies of the kinetics of SOFC reduction [51], its operation in open circuit conditions [50] as well as under current load [53], but all the studies mentioned were conducted using electrolyte-supported cells. In this work with studied anode-supported SOFCs with thin-film solid electrolyte membrane to carry the comparison out.

2. Experimental

2.1. Experimental techniques

The microstructure of ceramic layers of multilayered model SOFC samples was studied using a scanning electron microscope (SEM) LEO Supra 50VP with a field emitting cathode and INCA Energy + system of energy-dispersive X-ray microanalysis. Part of SEM images was also obtained using Dual Beam VERSA 3D HighVac (FEI) setup. Light transmission spectra of model samples were obtained using Specord M40 spectrometer (Carl Zeiss Jena, Germany) in a wavelength range from 200 to 900 nm.

2.2. Preparation of samples for transparency studies

In this work, we conducted a comparison study of model SOFCs based on thick single-crystal solid electrolyte and anode-supported cells with thin-film electrolyte prepared by magnetron sputtering. One needs to have an optically transparent solid electrolyte membrane in order to conduct Raman spectroscopy analysis of the inner interface between an anion conductor and anode electrode. That is why in previous work we conducted a study of the light transmission spectrum of 10Sc1YSZ solid electrolyte membrane with a thickness of 300 μm [54]. It was shown that in the studied region of wavelength (532–600 nm) this membrane has an energy transmission of about 70%, this value corresponds to the average window glass. In this work, we conducted a comparative analysis of energy transmission for 8YSZ single-crystal membrane and the same membrane with thin-film 8YSZ layers magnetron sputtered on it.

YSZ thin films were deposited by reactive pulsed dual magnetron sputtering on YSZ membranes. Two 6-mm-thick Zr/Y (85/15 at.%) targets with the size of 300 × 100 mm^2 were used. Prior to deposition, the substrates were ultrasonically cleaned sequentially in pure isopropyl alcohol, acetone, and distilled water. Before deposition, a vacuum chamber was evacuated to a base pressure of 10^{-3} Pa. The substrates were heated up to 300 °C. After that ion beam treatment of the substrate surface was performed for 10 min at a discharge voltage of 2 kV and discharge current of 100 mA, using an ion source with closed electron drift. Films were deposited in argon and oxygen mixture at operating pressure of 0.3 Pa. The thin film deposition rate was about 0,75 μm/h.

As a result of depositions, we prepared solid electrolyte membranes with thin-film electrolyte with a thickness of 1.6, 3 and 4.7 μm. Transparency investigations were done on both deposited films as it is and annealed in the air at 1100 °C.

2.3. Preparation of model SOFC samples

In this work we prepared two types of model solid oxide fuel cells samples: based on thick single-crystal solid electrolyte membrane and anode-supported cells based on commercially available SOFCMAN (China) anode supports.

2.3.1. Electrolyte-supported samples

Single crystalline 8YSZ (92 mol% ZrO_2 + 8 mol% Y_2O_3) solid electrolyte was prepared using a skull-melting technique in cold container [55,56]. Despite solid solutions doped with 10 mol% of Scandia and 1 mol% of Yttria (Ceria) show the highest ionic conductivity [57–59], we used 8YSZ composition as it has more simple Raman spectrum [60,61] and it is easy to separate the line of interest (Ce-O-Ce) from the total one. Solid electrolyte membranes (250 μm-thick disks with a diameter of 21 mm) were cut from single crystals in Institute of Solid State Physics RAS, obtained plates were polished.

Multilayered electrode deposition was optimized in previous works [62–65], all the electrode sublayers were deposited via screen-printed technique with intermediate dryings in the air at 130 °C and consecutive firing at elevated temperatures, active area of both electrodes was about 0.88 cm^2. Cathode electrode was based on LSM/10Sc1CeSZ composite materials (= 60/40 mass%) and fired in the air at 1100 °C for 2 h. Form of cathode electrode with a pinhole gave an opportunity to pass the excitation radiation on the inner interface between anode and electrolyte and get scattered radiation from the same point.

As for an anode electrode, an additional GDC layer was introduced in construction to precisely study the dependence of oxygen partial pressure as there is a line in doped ceria Raman spectrum which is significantly sensitive to oxygen stoichiometry inside the crystal lattice [66]. Anode layer consisted of 2 sublayers: functional and current-collecting ones. The functional layer was prepared of NiO/GDC (= 50/50 mass%) composite, each component was pre-fired at 700 °C in the air in order to achieve a proper morphology of grains [64]. The current-collecting anode was composed of NiO/10Sc1CeSZ (= 60/40 mass%) composite material, each component was pre-fired at 1100 °C in the air. All three sub-layers mentioned above were co-fired in the air at 1300 °C for 2 h. Both electrodes were coated with a platinum contact layer deposited via screen-printed technique consecutively fired in the air at 900 °C. Total scheme of layers' preparation routine for electrolyte-supported model solid oxide fuel cells is indicated in Table 1 (column “ESC”).

2.3.2. Anode-supported samples

Anode-supported model solid oxide fuel cells were based on commercially available SOFCMAN 2-layered anode supports with the thickness of 350 μm and diameter of 21 mm. We deposited 2-layered electrolyte – indicative GDC and YSZ – by means of magnetron sputtering technique. YSZ and GDC thin films were deposited by reactive pulsed dual magnetron sputtering on porous NiO/YSZ substrates. 6-mm-thick Zr/Y (85/15 at.%) and Ce/Gd (90/10 at.%) targets with the size of 300 × 100 mm^2 each were used. Other deposition parameters were the same as it was described in Section 2.2 regarding the preparation of samples for transparency studies. YSZ and GDC films were synthesized at a deposition rate of 0,75 μm/h and 1,7 μm/h, correspondingly.

Cathode layers, as well as platinum contact layers, were deposited following the same routine as we used for electrolyte-supported SOFCs, active area of cathode electrode was about 0.88 cm^2. Total scheme of layers' preparation routine for anode-supported model solid oxide fuel

Table 1
Preparation routine for electrolyte-supported (ESC) and anode-supported (ASC) solid oxide fuel cell model samples.

Layer	Sublayer	Composition, firing conditions (if applicable)	
		ESC	ASC
Cathode	Contact	Pt, screen-printed, 900 °C, 1 h Annealing	
	Functional	LSM/10Sc1CeSZ = 60/40, screen-printed, 1100 °C, 2 h	
Electrolyte		8SYZ, scull-melted, single crystalline, 250 μm	8SYZ, magnetron sputtered, ceramic, 5 μm
Anode	Indicative	GDC, screen-printed, 1300 °C, 2 h	GDC, magnetron sputtered, 3 μm
	Functional	NiO/GDC = 50/50, screen-printed, 1300 °C, 2 h	SOFCMAN 2-layered support, 350 μm
	Current-collecting	NiO/10Sc1CeSZ = 60/40, screen-printed, 1300 °C, 2 h	
	Contact	Pt, screen-printed, 900 °C, 1 h	

cells is indicated in Table 1 (column "ASC").

2.4. The combined setup of optical and electrochemical measurements

In this work, we used combined setup, which gives an opportunity to conduct simultaneous studies by means of traditional electrochemical techniques (studies of I-V curves, impedance spectroscopy, chronopotentiometry) and Raman spectroscopy. This combined setup was described in details is previous works [49–52]. The setup used in the current work consists of two main parts. First part gives opportunity to create SOFC working conditions: working temperature up to 1000 °C; air as oxidation atmosphere; controlled fuel atmosphere as mixture of hydrogen, nitrogen, carbon monoxide, methane, hydrogen sulfide; potentiostat-galvanostat to control a current load as well as impedance spectrometer to study a structure of model SOFCs' complex resistance. The second part of the setup gives the opportunity to create excitation radiation (semiconductor laser with the wavelength of 532 nm and power of 20 mW) and to collect Raman spectra from a selected point on SOFC model sample for selected operating conditions.

2.5. A routine of Raman spectra processing

As it was mentioned above, we applied an additional GDC layer in order to follow the changes in oxygen chemical potential by means of the intensity of Ce-O-Ce peak (~460 cm^{-1}) in GDC spectrum as the intensity of the line strongly depends on oxygen stoichiometry in crystal lattice [66].

Routine for Raman spectra processing was also described in details in previous works [67,68]. First of all, we applied the cyclic accumulation (100 cycles, 1 s with opened shutter and 1 s with closed shutter) of the signal to overcome the influence of the heat radiation effect. As the second step of processing, we applied a correction to the temperature-frequency factor and normalization on integral under the spectrum curve to take into account an influence of operating temperature. The third step of processing is a decomposition of spectra into components to separate the Ce-O-Ce (~460 cm^{-1}) peak, as we follow the dependence of this peak intensity on fuel mixture composition, a current load applied as well as operating temperature. Dependence of Ce-O-Ce on SOFC working conditions was used in this work to study the electrochemical parameters, e.g. local overpotential on the anode electrode.

3. Results and discussion

3.1. Light transmission studies and model sample microstructure

In this work we studied the transmission of light through 8YSZ single-crystalline plate with the thickness of 300 μm in comparison to the transmission of the same plate with thin-film YSZ layered deposited by means of magnetron sputtering technique for different thicknesses as well as annealed in the air at 1100 °C.

Transmission spectra for all the range of wavelength studied are presented in Fig. 1a. One can observe the transmission spectrum of start 8YSZ single-crystalline plate – black solid line. In a wavelength region studied further (indicated with black rectangular) – 532–600 nm – this plate has a transition ratio on a level of window glass (more than 70%). Introduction of thin-film magnetron sputtered 8YSZ layers (1.6 μm – red dashed line, 3.0 μm – green dotted line, 4.7 μm – blue dash-dotted line) effects the transition dependence mainly in a shortwave region (200–450 nm), we explain this influence by poor crystallinity of deposited film. Influence of thin-film thickness is monotonous and especially notable in a shortwave region. Influence of films deposited in working range of wavelength is rather low. Hence, we can use thin-film electrolyte deposited by means of magnetron sputtering in order to pass the excitation radiation and get a Raman scattered signal from the inner interface of solid electrolyte and anode electrode.

We also studied the influence of thin-film annealing in the air at 1100 °C (Fig. 1, magenta dash-dot-dotted line). One can observe that annealing lowers the influence of film on light transition, which corresponds to the crystallization of the film in the course of high-temperature annealing.

One can observe from Fig. 1a, that intensity curves have oscillating nature. This effect is even more periodic on the dependence on wavenumber – Fig. 1b. We explain this periodic structure by interference effect in a thin-film. For light beams, which are perpendicular to the surface of 8YSZ plate path difference is:

$$\Delta = 2nd, \tag{1}$$

where n is the refractive index of thin-film, and d is its thickness. Maximums of intensity corresponding to the path difference equal to an integer number of wavelength:

$$\Delta = 2\mathrm{nd} = \mathrm{m}\lambda = \frac{m}{k}, \tag{2}$$

where m is integer number, λ is wavelength, k is wavenumber. Thus maximums of intensity happen for following wavenumbers:

$$k = \frac{m}{2nd} \tag{3}$$

For the case of the periodic picture of intensity depending on wavenumber k with the period of Δk one can estimate a refractive index of the film:

$$n = \frac{1}{2d\Delta k} \tag{4}$$

Results for such estimation for our interference pictures are presented in Table 2.

One can observe from data in Table 2, that resulting refractive indexes are equal for all the thicknesses studied, results obtained are close to literature data [69–71].

Layers' microstructure for model solid oxide fuel cells (electrolyte-supported and anode-supported) was studied by means of scanning electron microscopy imaging from cell cross-section. SEM image for the electrolyte-supported cell is shown in Fig. 2a. One can observe part of single-crystalline solid electrolyte membrane in the lower part of the image. Upper than membrane one can observe a thin-film indicative

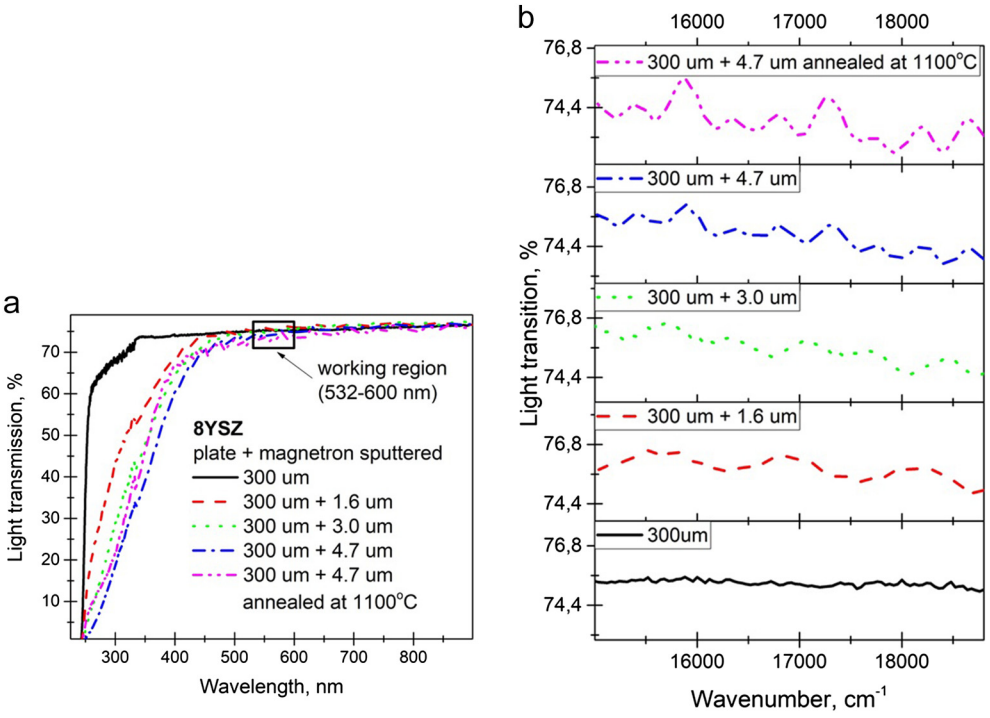

Fig. 1. a – Light transition spectra of clear (black) 300 μm thick single-crystal 8YSZ plate and covered by as-prepared thin-film magnetron sputtered 8YSZ-layer for different thicknesses (1.6 μm – dashed red, 3.0 μm – doted green, 4.7 μm – dash-doted blue) as well as annealed in the air at 1100 °C (4.7 μm – dash-double-doted magenta); b – same light transition spectra in dependence on wavenumber in studied region. (For interpretation of the references to color in this figure legend, the reader is referred to the web version of this article.)

Table 2
Results for 8YSZ thin-film layer refractive index estimated from interference picture – periodic change in light transition in dependence on wavenumber.

Thin-film thickness – *d*, μm	Δ*k*, cm^{-1}	Refractive index, *n*
1.6	1225 ± 40	2.5 ± 0.1
3.0	660 ± 40	2.5 ± 0.2
4.7	445 ± 40	2.4 ± 0.2

GDC layer with the thickness of about 2–3 μm. Porous functional anode layer is deposited on GDC layer and has a thickness of about 8 μm, a boundary is quite clear, sublayer consists of submicron size particles. Current-collecting anode layer has a significantly larger size of particles and pores – of about 1–2 μm, its thickness of a bit more than 10 μm. Contact platinum layer can be observed in the upper part of the image.

SEM image of anode-supported cell cross-section is shown in Fig. 2b. Anode layer (support in this case) is once again shown in the upper part of the figure, it consists of submicron-sized particles, pores have close size. Thin-film indicative GDC layer was deposited on anode supports, it is lightest on this image, has a thickness of about 2–3 μm. 8YSZ sublayer was also deposited by magnetron sputtering, it is clearly gas-tight and has a thickness of about 5 μm. Porous cathode electrode can be observed in the bottom part of the image, particles have a submicron size.

3.2. Electrochemical performance of model SOFCs

Electrochemical performance of model SOFCs with electrolyte and anode support was tested using studies of I-V and power curves, as well as by means of impedance spectroscopy. I-V and power curves of cells with different support types obtained at 750 °C for different fuel gas mixtures are shown in Fig. 3a. One can observe the quite low value of the open-circuit voltage of anode-supported cells (about 0.93 V). Meanwhile, OCV for electrolyte-supported fuel cells is more than 1 V for both fuel mixtures. This fact is direct evidence of the existence of gas or electron leakages in thin-film solid electrolyte membrane of anode-supported SOFCs. In current work, we used model anode-supported solid oxide fuel cells with a 2-layered GDC/YSZ solid electrolyte. Unlike ordinary ASC in order to create oxygen chemical potential probe in

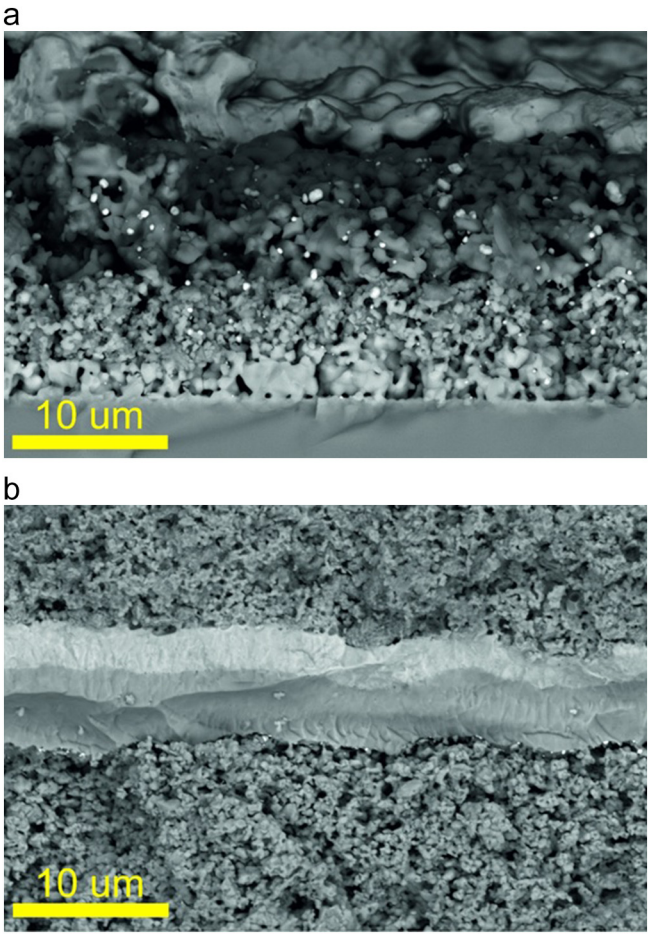

Fig. 2. a – SEM image of the cross-section of electrolyte-supported model solid oxide fuel cell; b – SEM image of the cross-section of anode-supported model solid oxide fuel cell.

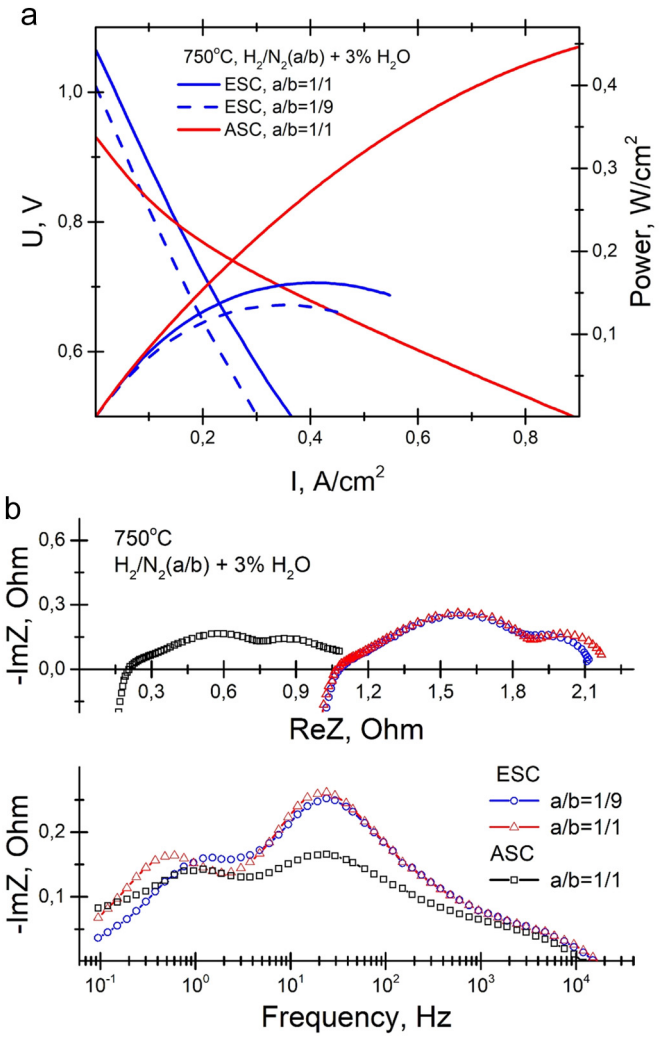

Fig. 3. a – I-V and power curves for electrolyte (blue) and anode-supported (red) solid oxide fuel cells for different fuel mixtures: solid lines – H_2/N_2 = 1/1, dashed line – H_2/N_2 = 1/9. b – Impedance spectra for same model SOFCs and same fuel compositions. (For interpretation of the references to color in this figure legend, the reader is referred to the web version of this article.)

developed samples anode support was covered by GDC layer firstly. Ceria is well known for its significant dependence of conducting and thermomechanical properties on oxygen partial pressure in the surrounding atmosphere. By reason of poor stability of thin-film membrane, we could not work with an anode-supported structure in a wide range of oxygen partial pressures. The influence of different fuel gas mixtures was studied only for electrolyte-supported solid oxide fuel cells.

One can also see from Fig. 3a, that power density for anode-supported cells exceeds a value of 0.45 W/cm^2 meanwhile corresponding value for electrolyte-supported structures is less than 0.2 W/cm^2. Impedance spectra of ESC and ASC SOFCs are presented in Fig. 3b. One can observe, that anode-supported fuel cell has a significantly lower value of total resistance, than corresponding values for electrolyte-supported sample. Ohmic part of impedance spectra differs more significantly for cells with a different type of support, polarization part is close for different support types. It is obvious from the impedance spectrum of the electrolyte-supported fuel cell, that about half of total resistance is caused by ohmic loses on anion transport in the solid electrolyte membrane. This fact explains the lowering of total resistance after the switch to anode-supported structure: thin-film electrolyte has a significantly lower thickness and ohmic resistance. As for the dependence of I-V and power curves of ESC SOFCs on fuel composition, a ratio of hydrogen to nitrogen partial pressures mainly influences an OCV value and diffusion part of total resistance (Fig. 3b).

3.3. Analysis of Raman spectra of model SOFCs

Fig. 4a shows room temperature Raman spectra obtained from inner interface “anode | electrolyte” of electrolyte-supported (bottom curve) and anode-supported (top curve) model solid oxide fuel cells. Majority of peaks obtained were identified in accordance with Raman spectra of zirconia, ceria and nickel oxide known from the literature data. Raman peaks with shifts of 170, 260, 340, 570 and 610 cm^{-1} can be attributed to the structure of cubic zirconia [55]. These peaks can be explained by the influence of single-crystalline thick solid electrolyte membrane in a case of electrolyte-supported structures and by thin-film polycrystalline 8YSZ membrane deposited by magnetron sputtering in a case of anode-supported structures. Despite of polycrystalline nature of ASC thin-film electrolyte, an influence of 8YSZ on Raman spectra obtained for ESC structures is much higher due to large thickness of the single-crystalline support membrane.

Raman peaks with shifts of 680 and 900 cm^{-1} correspond to nickel oxide present in the functional anode layer [72]. It is quite obvious, that nickel oxide Raman lines are noticeable in significantly higher degree for anode-supported structure. This result can be explained by two factors: the usage of thin-film solid electrolyte with the lower influence of 8YSZ on total Raman spectrum of ASC sample and higher transparency of GDC layer deposited by means of magnetron sputtering in comparison of screen-printed one in case of thick electrolyte support. Quite intense Raman peak with the shift of about 470 cm^{-1} can be attributed to doped ceria GDC indicative sublayer [66]. Further studies of Raman spectra obtained from the inner interface of the anode electrode and solid electrolyte membrane were carried out in reducing conditions.

Fig. 4b shows the evolution of Raman spectra after application of working temperature – 750 °C. One can observe that relative intensity of peaks corresponding to GDC lowers due to the switching to reducing atmosphere. Moreover, Raman spectra become more complex because of the influence of heat radiation. Despite the complexity of presented spectra, one can observe the change of Raman spectrum intensity in the course of change of fuel mixture composition. All changes happen in the vicinity of Raman peak with the shift of about 460 cm^{-1} (this peak corresponds to doped ceria, it is significantly sensitive to oxygen stoichiometry inside the crystal lattice [66]). Decrease of the hydrogen partial pressure in a fuel gas mixture with a constant humidity causes an increase of the oxygen partial pressure and oxygen stoichiometry in GDC material and, as a result, the intensity of corresponding peak increases. Despite all the spectra presented in Fig. 4b were normalized by frequency-temperature factor and by the total integral of the spectrum, one needs to perform a decomposition of spectra in order to separate the line of interest (~460 cm^{-1}) and analyze its intensity. We used a procedure of spectra processing described in Section 2.5.

Results of line separation are presented in Fig. 4c. One can observe a clear dependence of peak intensity on oxygen partial pressure: line intensity increases when oxygen partial pressure increases. We connect this change with the growth of oxygen content inside the doped ceria crystal lattice and thus increase of probability of Raman scattering on O-Ce-O lattice oscillations. Dependence with the same character was detected for the case of current load application. Raman peak intensity growth after application of the current load, the higher the current – the higher is peak intensity. This effect can be explained by the transfer of oxygen anion from the electrolyte membrane to the lattice of indicative GDC sublayer.

Raman spectra measurements were made in two main regimes: in variable fuel gas mixtures at OCV conditions, when it could be assumed that GDC layer is in thermodynamic equilibrium with fuel atmosphere; under variable current load at fixed fuel gas mixture. Results are

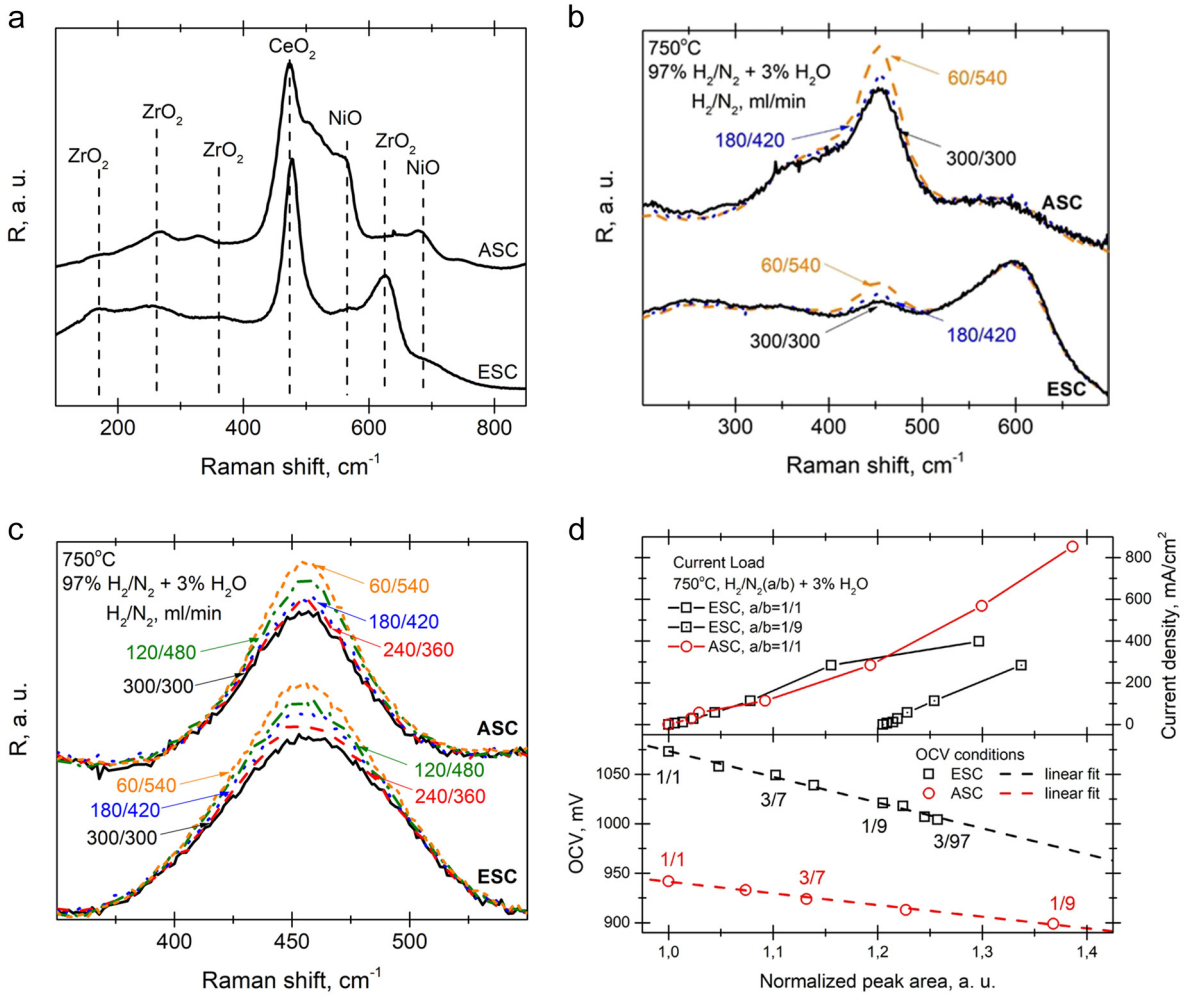

Fig. 4. a – Comparison of room temperature spectra for electrolyte- and anode-supported cells with identification of Raman peaks known from literature data. b – A variation of Raman spectra under change of fuel mixture composition. c – A result of the line of interest (~460 cm^{-1}) separation from Raman spectra in dependence on fuel mixture composition. d – Dependence of open-circuit voltage (OCV) and current density on normalized peak area for the line of interest (~460 cm^{-1}).

presented in Fig. 4d, all intensities are normalized on the intensity of corresponding spectra measured under OCV conditions and fuel gas mixture 97% H_2/N_2 (1,1) +3% H_2O. It worth noting again, that thin film membrane of anode-supported fuel cells were not sufficiently stable and thus these cells were measured for only one fuel mixture composition with equal partial pressures of hydrogen and nitrogen.

As can be seen in Fig. 4d (bottom), dependences of OCV on peak area are linear like both for ASC and ESC samples. Assuming local thermodynamical equilibrium on SOFC anode electrode in case of zero currents passing through the cell, one can evaluate a linear connection between changes in 460 cm^{-1} peak area and level of oxygen chemical potential in the region of inner "anode | electrolyte" interface. This procedure was applied to the sets of data obtained at constant fuel gas mixture and various current load presented on Fig. 4d (top). The result of calculated anode overpotential is presented in Fig. 5a.

Fuel gas content and type of the studied SOFC has practically no influence on obtained anode overpotential up to the 150 mA/cm^2 current load. As for higher current loads overpotential dependence shows significant difference for different types of cells. On Fig. 5b there is an anode part of impedance spectra obtained by subtraction of cathodic (measured by means of the potential electrode) impedance spectra from the whole impedance spectra of electrolyte supported samples measured at 2 different fuel gas mixture contents. It is clear from presented spectra, that percent of hydrogen in anode atmosphere influences only on a low-frequency part of anodic impedance spectra ($R_{l.f.}$), corresponding to slow diffusive electrode processes. The medium ($R_{m.f.}$, catalytic processes) and high ($R_{h.f.}$, ohmic losses) frequency parts show no changes but differ from each other more than 5 times in amplitude. Calculated "catalytic" overpotential with a constant slop equal to the resistance of medium frequency part ($R_{m.f.}$) of the anodic impedance spectra presented on Fig. 5a by the dashed blue line is in a good agreement with values of anode overpotential evaluated from Raman spectroscopy of inner "anode | electrolyte" interface.

4. Conclusions

In presented work, the possibility of application of in-situ Raman spectroscopy of inner interfaces of SOFC with ceramic thin-film electrolyte was shown. Investigation of transparency spectra of single-crystal plates with and without thin films deposited by magnetron sputtering showed no significant influence on transparency level in working region and refractive index evaluated from observed interference picture was in a good agreement with literature data for all investigated films. It was shown that adding of GDC-indicative layer gives a possibility to conduct an in-situ investigation of oxygen chemical potential on inner "anode | electrolyte" interface over current load or fuel gas mixture, but double-layered GDC/YSZ thin-film electrolyte shows the presence of electronic or gas leakages due to poor stability in reduction atmosphere. Despite significantly low inner resistance in comparison to ESC, the quality of ASC thin-film membrane

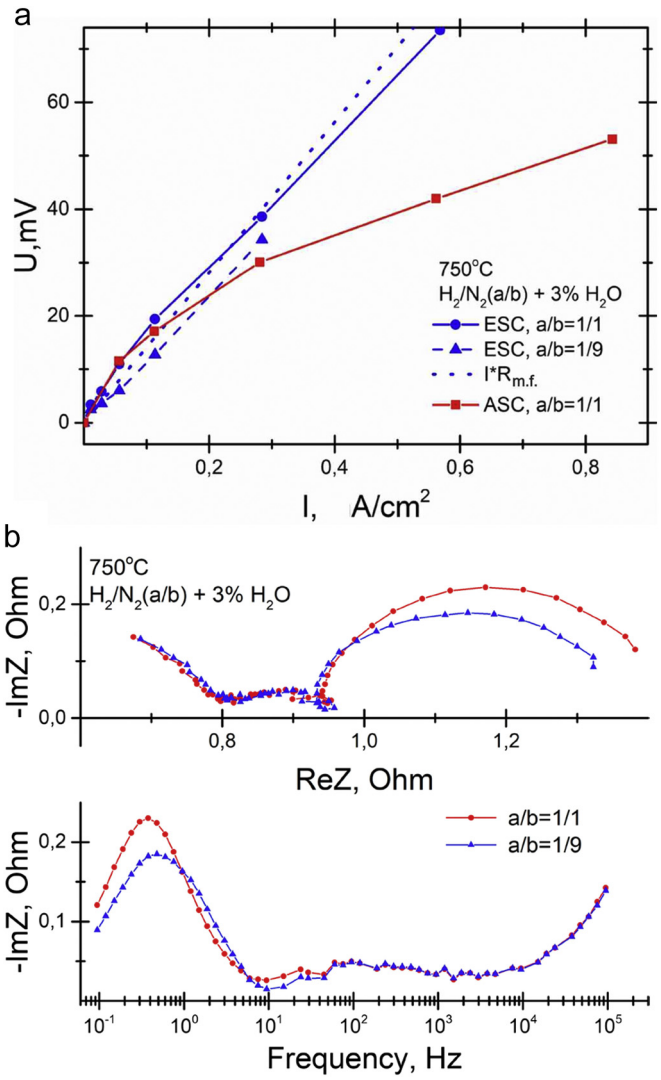

Fig. 5. a – Calculated anodic overpotential for electrolyte- and anode-supported model SOFCs. b – Anode part of impedance spectra obtained by subtraction of cathodic (measured by means of the potential electrode) impedance spectra from the whole impedance spectra of electrolyte supported samples measured at 2 different fuel gas mixture contents.

strongly limits temperature, current load, and fuel content investigation ranges. Application of thin-film membranes significantly lowers the influence of 8YSZ on Raman spectra of inner "anode | electrolyte" interface. After post-processing and normalization, the obtained Raman spectra show similar influence on the area of the GDC 460 cm^{-1} peak of current load value or hydrogen content in fuel gas mixture. The linear dependence of OCV on 460 cm^{-1} peak area makes it possible to evaluate an easy connection between Raman GDC peak area changes and evolution of the oxygen chemical potential insight the anode electrode under current load. Comparative analysis of anodic impedance under different fuel gas mixtures allows us to assume that spectroscopic measurements of inner interfaces give direct information about the contribution of the fuel oxidation reaction to the total SOFC losses.

Acknowledgments

Financial support from the Russian Science Foundation project 17-79-30071 "Scientifically grounded optimization of power and mass-dimensional characteristics of planar SOFC stacks and development of fuel processor for highly-efficient transport and stationary power plants" is gratefully acknowledged for the part of studies performed with electrolyte-supported model SOFCs. Authors would like to thank a Russian President Grant MK-1998.2019.2 "In-situ studies of current-generating reactions in electrodes of solid oxide fuel cells (SOFC) with thin-film electrolyte by means of Raman spectroscopy (RS)" for financial support of studies of anode-supported model solid oxide fuel cells.

References

[1] N. Mahato, A. Benerjee, A. Gupta, S. Omar, K. Balani, Progress in material selection for solid oxide fuel cell technology: a review, Prog. Mater. Sci. 72 (2015) 141–337, https://doi.org/10.1016/j.pmatsci.2015.01.001.
[2] E.D. Wachsman, K.T. Lee, Lowering the temperature of solid oxide fuel cells, Science 334 (2011) 935–939, https://doi.org/10.1126/science.1204090.
[3] E.D. Wachsman, C.A. Marlowe, K.T. Lee, Role of solid oxide fuel cells in a balanced energy strategy, Energy Environ. Sci. 5 (2012) 5498–5509, https://doi.org/10.1039/C1EE02445K.
[4] F.A. Al-Sulaiman, I. Dincer, F. Hamdullahpur, Exergy analysis of an integrated solid oxide fuel cell and organic Rankine cycle for cooling, heating and power production, J. Power Sources 195 (2010) 2346–2353, https://doi.org/10.1016/j.jpowsour.2009.10.075.
[5] A. Choudhury, H. Chandra, A. Arora, Application of solid oxide fuel cell technology for power generation—a review, Renew. Sust. Energ. Rev. 20 (2013) 430–442, https://doi.org/10.1016/j.rser.2012.11.031.
[6] P.V. Snytnikov, S.D. Badmaev, G.G. Volkova, D.I. Potemkin, M.M. Zyryanova, V.D. Belyaev, V.A. Sobyanin, Catalysts for hydrogen production in a multifuel processor by methanol, dimethyl ether and bioethanol steam reforming for fuel cell applications, Int. J. Hydrog. Energy 37 (2012) 16388–16396, https://doi.org/10.1016/j.ijhydene.2012.02.116.
[7] A.V. Samoilov, D.A. Agarkov, S.I. Bredikhin, A multifuel processor for SOFC power plants created to operate in the Arctic region, ECS Trans. 91 (2019) (accepted).
[8] W. Wang, C. Su, Yu. Wu, R. Ran, Z. Shao, Progress in solid oxide fuel cells with nickel-based anodes operating on methane and related fuels, Chem. Rev. 113 (2013) 8104–8151, https://doi.org/10.1021/cr300491e.
[9] M. Pillai, Y. Lin, H. Zhu, R.J. Kee, S.A. Barnett, Stability and coking of direct-methane solid oxide fuel cells: effect of CO_2 and air additions, J. Power Sources 195 (2010) 271–279, https://doi.org/10.1016/j.jpowsour.2009.05.032.
[10] R.-U. Dietrich, J. Oelze, A. Lindermeir, C. Spitte, M. Steffen, T. Küster, S. Chen, C. Schlitzberger, R. Leithner, Efficiency gain of solid oxide fuel cell systems by using anode offgas recycle – results for a small scale propane driven unit, J. Power Sources 196 (2011) 7152–7160, https://doi.org/10.1016/j.jpowsour.2010.09.016.
[11] L. Zhang, C. Yang, A.I. Frenkel, S. Wang, G. Xiao, K. Brinkman, F. Chen, Co-generation of electricity and chemicals from propane fuel in solid oxide fuel cells with anode containing nano-bimetallic catalyst, J. Power Sources 262 (2014) 421–428, https://doi.org/10.1016/j.jpowsour.2014.04.009.
[12] H. Sumi, T. Yamaguchi, K. Hamamoto, T. Suzuki, Y. Fujishiro, Impact of direct butane microtubular solid oxide fuel cells, J. Power Sources 220 (2012) 74–78, https://doi.org/10.1016/j.jpowsour.2012.07.106.
[13] Y. Wang, L. Sun, L. Luo, Y. Wu, L. Liu, J. Shi, The study of portable direct-flame solid oxide fuel cell (DF-SOFC) stack with butane fuel, J. Fuel Chem. Tech. 42 (2014) 1135–1139, https://doi.org/10.1016/S1872-5813(14)60045-1.
[14] S.D. Badmaev, A.A. Pechenkin, V.D. Belyaev, S.A. Ven'yaminov, P.V. Snytnikov, V.A. Sobyanin, V.N. Parmon, Steam reforming of dimethoxymethane to hydrogen-rich gas for fuel cell feeding application, Dokl. Phys. Chem. 452 (2013) 251–253, https://doi.org/10.1134/S0012501613100060.
[15] M.M. Zyraynova, P.V. Snytnikov, Yu.I. Amosov, V.D. Belyaev, V.V. Kireenkov, V.A. Kuzin, M.V. Vernikovskaya, V.A. Kirillov, V.A. Sobyanin, Upgrading of associated petroleum gas into methane-rich gas for power plant feeding applications. Technological and economic benefits, Fuel 108 (2013) 282–291, https://doi.org/10.1016/j.fuel.2013.02.047.
[16] A.A. Pechenkin, S.D. Badmaev, V.D. Belyaev, E.A. Paukshtis, O.A. Stonkus, Sobyanin, Steam Reforming of Dimethoxymethane, Methanol and Dimethyl Ether on CuO–ZnO/γ-Al2O3 Catalyst, Kinet. Catal. 58 (2017) 577–584, https://doi.org/10.1134/S0023158417050196.
[17] E.M. Churakova, S.D. Badmaev, P.V. Snytnikov, A.I. Gubanov, E.Y. Filatov, P.E. Plyusnin, V.D. Belyaev, S.V. Korenev, V.A. Sobyanin, Bimetallic Rh-Co/ZrO_2 catalysts for ethanol steam reforming into hydrogen-containing gas, Kinet. Catal. 51 (2010) 893–897, https://doi.org/10.1134/S0023158410060157.
[18] S.D. Badmaev, P.V. Snytnikov, Hydrogen production from dimethyl ether and bioethanol for fuel cell applications, Int. J. Hydrog. Energ. 33 (2008) 3026–3030, https://doi.org/10.1016/j.ijhydene.2008.02.016.
[19] V.N. Rogozhnikov, N.A. Kuzin, P.V. Snytnikov, D.I. Potemkin, T.B. Shoynkhorova, P.A. Simonov, V.A. Shilov, N.V. Ruban, A.V. Kulikov, V.A. Sobyanin, Design, scale-up, and operation of a Rh/Ce0.75Zr0.25O2-δ-η-Al2O3/FeCrAl alloy wire mesh honeycomb catalytic module in diesel autothermal reforming, Chem. Eng. J. 374 (2019) 511–519, https://doi.org/10.1016/j.cej.2019.05.205.
[20] A.V. Samoilov, V.A. Kirillov, A.B. Shigarov, A.S. Brayko, D.I. Potemkin, T.B. Shoikhorova, P.V. Snytnikov, S.I. Uskov, A.A. Pechenkin, V.D. Belyaev, V.A. Sobyanin, Prereforming of Arctic diesel fuel into syngas, Catal. Ind. 10 (2018) 321–327, https://doi.org/10.1134/S207005041804013X.
[21] E. Açıkkalp, Performance analysis of irreversible solid oxide fuel cell – Brayton heat engine with ecological based thermo-environmental criterion, Energ. Conv. Manag. 148 (2017) 279–286, https://doi.org/10.1016/j.enconman.2017.06.003.

[22] Y. Casas, J. Dewulf, L.E. Arteaga-Pérez, M. Morales, H.V. Langenhove, E. Rosa, Integration of solid oxide fuel cell in a sugar–ethanol factory: analysis of the efficiency and the environmental profile of the products, J. Clean. Prod. 19 (2011) 1395–1404, https://doi.org/10.1016/j.jclepro.2011.04.018.

[23] N.P. Brandon, E. Ruiz-Trejo, P. Boldin, Solid Oxide Fuel Cell Lifetime and Reliability. Critical Challenges of Fuel Cells, Academic Press, 2017.

[24] P. Hofmann, A. Schweiger, L. Fryda, K.D. Panopoulos, U. Hohenwarter, J.D. Bentzen, J.P. Ouweltjes, J. Ahrenfeldt, U. Henriksen, E. Kakaras, High temperature electrolyte supported Ni-GDC/YSZ/LSM SOFC operation on two-stage Viking gasifier product gas, J. Power Sources 173 (2007) 357–366, https://doi.org/10.1016/j.jpowsour.2007.04.073.

[25] Q. Ma, F. Tietz, A. Leonide, E. Ivers-Tiffée, Anode-supported planar SOFC with high performance and redox stability, Electrochem. Commun. 12 (2010) 1326–1328, https://doi.org/10.1016/j.elecom.2010.07.011.

[26] T.-H. Lim, R.-H. Song, D.-R. Shin, J.-I. Yang, H. Jung, I.C. Vinke, S.-S. Yang, Operating characteristics of a 5 kW class anode-supported planar SOFC stack for a fuel cell/gas turbine hybrid system, Int. J. Hydrog. Energ. 33 (2008) 1076–1083, https://doi.org/10.1016/j.ijhydene.2007.11.017.

[27] X.J. Chen, Q.L. Liu, S.H. Chan, N.P. Brandon, K.A. Khor, High-performance cathode-supported SOFC with perovskite anode operating in weakly humidified hydrogen and methane, Fuel Cells Bull 2007 (2007) 12–16, https://doi.org/10.1016/S1464-2859(07)70261-4.

[28] Y. Liu, S.-I. Hashimoto, H. Nishino, K. Takei, M. Mori, T. Suzuki, Y. Funahashi, Fabrication and characterization of micro-tubular cathode-supported SOFC for intermediate temperature operation, J. Power Sources 174 (2007) 95–102, https://doi.org/10.1016/j.jpowsour.2007.08.101.

[29] S. Hui, D. Yang, Z. Wang, S. Yick, C. Decès-Petit, W. Qu, A. Tuck, R. Maric, D. Ghosh, Metal-supported solid oxide fuel cell operated at 400–600 °C, J. Power Sources 167 (2007) H336–339, https://doi.org/10.1016/j.jpowsour.2007.02.070.

[30] M.C. Tucker, G.Y. Lau, C.P. Jacobson, L.C. DeJonghe, S.J. Visco, Performance of metal-supported SOFCs with infiltrated electrodes, J. Power Sources 171 (2007) 477–482, https://doi.org/10.1016/j.jpowsour.2007.06.076.

[31] D. Panthi, B. Choi, A. Tsutsumi, Fabrication and evaluation of a micro-tubular solid oxide fuel cell with an inert support using scandia-stabilized zirconia electrolyte, J. Electrochem. Soc. 162 (2015) F1555–F1560, https://doi.org/10.1149/2.1031514jes.

[32] K. Zhao, B.-H. Kim, Q. Xu, B.-G. Ahn, Fabrication and characterization of inert-substrate-supported tubular single cells by dip-coating process, J. Power Sources 245 (2014) 671–677, https://doi.org/10.1016/j.jpowsour.2013.07.022.

[33] N.B. Colthup, L.H. Daly, S.E. Wiberley, Introduction to Infrared and Raman Spectroscopy, 2nd edition, Academic Press, 1975.

[34] J.R. Ferraro, K. Nakamoto, C.W. Brown, Introductory Raman Spectroscopy, 2nd edition, Academic Press, 1977.

[35] M.B. Pomfret, J.C. Owrutsky, R.A. Walker, High-temperature Raman spectroscopy of solid oxide fuel cell materials and processes, J. Phys. Chem. B 110 (2006) 17305–17308, https://doi.org/10.1021/jp063952l.

[36] X. Li, J.-P. Lee, K.S. Blinn, D. Chen, S. Yoo, B. Kang, L.A. Bottomley, M.A. El-Sayed, S. Park, M. Liu, High-temperature surface enhanced Raman spectroscopy for in situ study of solid oxide fuel cell materials, Energy Environ. Sci. 7 (2014) 306–310, https://doi.org/10.1039/C3EE42462F.

[37] K.S. Blinn, H. Abernathy, X. Li, M. Liu, L.A. Bottonley, M. Liu, Raman spectroscopic monitoring of carbon deposition on hydrocarbon-fed solid oxide fuel cell anodes, 7 (2012) 7913–7917, https://doi.org/10.1039/C2EE21499G.

[38] M.B. Pomfret, J. Marda, G.S. Jackson, B.W. Eichhorn, A.M. Dean, R.A. Walker, Hydrocarbon fuels in solid oxide fuel cells: in situ Raman studies of graphite formation and oxidation, J. Phys. Chem. C 112 (2008) 5232–5240, https://doi.org/10.1021/jp711312p.

[39] M.B. Pomfret, J.C. Owrutsky, R.A. Walker, In situ studies of fuel oxidation in solid oxide fuel cells, Anal. Chem. 79 (2007) 2367–2372, https://doi.org/10.1021/ac062189o.

[40] B.C. Eigenbrodt, M.B. Pomfret, D.A. Steinhurst, J.C. Owrutsky, R.A. Walker, Direct, in situ optical studies of Ni − YSZ anodes in solid oxide fuel cells operating with methanol and methane, J. Phys. Chem. C 115 (2011) 2895–2903, https://doi.org/10.1021/jp109292r.

[41] Z. Cheng, M. Liu, Characterization of sulfur poisoning of Ni–YSZ anodes for solid oxide fuel cells using in situ Raman microspectroscopy, Solid State Ionics 178 (2007) 925–935, https://doi.org/10.1016/j.ssi.2007.04.004.

[42] A. Ishikura, S. Sakuno, N. Komiyama, H. Sasatsu, N. Masuyama, H. Itoh, K. Yasumoto, Influence of H2S poisoning on anode layer of SOFC, ECS Trans. 7 (2007) 845–850, https://doi.org/10.1149/1.2729174.

[43] F. Iguchi, S. Onodera, N. Sata, H. Yugami, Study of Raman peak shift under applied isostatic pressure in rare-earth-doped ceria for evaluation of quantitative stress conditions in SOFCs, Solid State Ionics 225 (2012) 99–103, https://doi.org/10.1016/j.ssi.2012.06.022.

[44] S. Onuki, S. Onodera, F. Iguchi, M. Shimizu, T. Kawada, H. Yugami, Evaluation of stress condition of operated anode supported-type SOFC under operating conditions based on Raman scattering spectroscopy, ECS Trans. 57 (2013) 951–957, https://doi.org/10.1149/05701.0951ecst.

[45] J.D. Kirtley, D.M. Halat, M.D. McIntyre, B.C. Eigenbrodt, R.A. Walker, High-temperature “spectrochronopotentiometry”: correlating electrochemical performance with in situ Raman spectroscopy in solid oxide fuel cells, Anal. Chem. 84 (2012) 9745–9753, https://doi.org/10.1021/ac301504g.

[46] J. Kirtley, A. Singh, D. Halat, T. Oswell, J.M. Hill, R.A. Walker, In situ Raman studies of carbon removal from high temperature Ni–YSZ cermet anodes by gas phase reforming agents, J. Phys. Chem. C 117 (2013) 25908–25916, https://doi.org/10.1021/jp408192e.

[47] E. Brightman, R. Maher, G.J. Offer, V. Duboviks, C. Heck, L.F. Cohen, Designing a miniaturised heated stage for in situ optical measurements of solid oxide fuel cell electrode surfaces, and probing the oxidation of solid oxide fuel cell anodes using in situ Raman spectroscopy, Rev. Sci. Instr. 83 (2012) 053707, , https://doi.org/10.1063/1.4719955.

[48] Agarkov, D.A., Bredikhin, S.I., Burmistrov, I.N., Kveder, V.V., Tsybrov, F.M. Patent RU161095U1.

[49] D.A. Agarkov, I.N. Burmistrov, F.M. Tsybrov, I.I. Tartakovskii, V.V. Kharton, S.I. Bredikhin, V.V. Kveder, Analysis of interfacial processes at the SOFC electrodes by in-situ Raman spectroscopy, ECS Trans. 68 (2015) 2093–2103, https://doi.org/10.1149/06801.2093ecst.

[50] D.A. Agarkov, I.N. Burmistrov, F.M. Tsybrov, I.I. Tartakovskii, V.V. Kharton, S.I. Bredikhin, In-situ Raman spectroscopy analysis of the interfaces between Ni-based SOFC anodes and stabilized zirconia electrolyte, Solid State Ionics 302 (2017) 133–137, https://doi.org/10.1016/j.ssi.2016.12.034.

[51] D.A. Agarkov, I.N. Burmistrov, F.M. Tsybrov, I.I. Tartakovskii, V.V. Kharton, S.I. Bredikhin, Kinetics of NiO reduction and morphological changes in composite anodes of solid oxide fuel cells: estimate using Raman scattering technique, Russ. J. Electrochem. 52 (2016) 600–605, https://doi.org/10.1134/S1023193516070028.

[52] Agarkov, D.A., Bredikhin, S.I., Burmistrov, I.N., Tartakovskii, I.I., Tsybrov, F.M. Patent RU165785U1.

[53] D.A. Agarkov, I.N. Burmistrov, F.M. Tsybrov, I.I. Tartakovskii, V.V. Kharton, S.I. Bredikhin, In-situ Raman spectroscopy analysis of the interface between ceria-containing SOFC anode and stabilized zirconia electrolyte, Solid State Ionics 319C (2018) 125–129, https://doi.org/10.1016/j.ssi.2018.02.006.

[54] D.A. Agarkov, Studies of Relation between Microstructure and Charge Transfer Processes in Planar SOFC Composite Electrodes, (2017) (PhD thesis). (Chernogolovka, Russia).

[55] M.A. Borik, E.E. Lomonova, V.V. Osiko, V.A. Panov, O.E. Porodinkov, M.A. Vishnyakova, Y. Voron’Ko, V.V. Voronov, Partially stabilized zirconia single crystals: growth from the melt and investigation of the properties, J. Cryst. Growth 275 (2005) e2173–e2179, https://doi.org/10.1016/j.jcrysgro.2004.11.244.

[56] V.I. Aleksandrov, V.P. Vojtsitskij, E.E. Lomonova, V.V. Osiko, N.P. Khaneev, Melt propagation control at initial stage of direct high-frequency melting in cool container, Prib. Tech. Eksp. 4 (1992) 212–217.

[57] D.A. Agarkov, M.A. Borik, S.I. Bredikhin, I.N. Burmistrov, G.M. Eliseeva, V.A. Kolotygin, A.V. Kulebyakin, I.E. Kuritsyna, E.E. Lomonova, F.O. Milovich, V.A. Myzina, P.A. Ryabochkina, N.Y. Tabachkova, T.V. Volkova, Structure and transport properties of zirconia crystals codoped by scandia, ceria and yttria, J. Mater. 5 (2019) 273–279, https://doi.org/10.1016/j.jmat.2019.02.004.

[58] F.O. Milovich, M.A. Borik, N.Y. Tabachkova, D.A. Agarkov, E.E. Lomonova, I.E. Kuritsyna, V.T. Bublik, V.A. Kolotygin, A.S. Chislov, A.V. Kulebyakin, V.A. Myzina, V.V. Osiko, Phase stability and transport characteristics of (ZrO2)1-x(Sc2O3)x(CeO2)y and (ZrO2)1-x-y-z(Sc2O3)x(CeO2)y(Y2O3)z solid solution crystals, J. All. Cmpd. 191 (2019) 445–451, https://doi.org/10.1016/j.jallcom.2019.03.263.

[59] D.A. Agarkov, M.A. Borik, S.I. Bredikhin, I.N. Burmistrov, A.S. Chislov, G.M. Eliseeva, V.A. Kolotygin, A.V. Kulebyakin, I.E. Kuritsyna, E.E. Lomonova, F.O. Milovich, V.A. Myzina, N. Yu Tabachkova, Transport properties of single crystals of solid electrolytes based on ZrO2-Sc2O3 co-doped by scandia, yttria, ytterbia and ceria, Chem. Prob. 2 (17) (2019) 235–245, https://doi.org/10.32737/2221-8688-2019-2-235-245.

[60] K. Nomura, Y. Mizutani, M. Kawai, Y. Nakamura, O. Yamamoto, Aging and Raman scattering study of scandia and yttria doped zirconia, Solid State Ionics 132 (2000) 235–239, https://doi.org/10.1016/S0167-2738(00)00648-2.

[61] D.A. Agarkov, E.A. Agarkova, M.A. Borik, S.I. Bredikhin, A.V. Kulebyakin, I.E. Kuritsyna, E.E. Lomonova, F.O. Milovich, V.A. Myzina, P.A. Ryabochkina, N.Y. Tabachkova, T.V. Volkova, Comparison of structural and transport properties of zirconia single-crystals stabilized by yttria and gadolinia, ECS Trans. 91 (2019) (accepted).

[62] I.N. Burmistrov, D.A. Agarkov, E.V. Korovkin, D.V. Yalovenko, S.I. Bredikhin, Fabrication of membrane-electrode assemblies for solid oxide fuel cells by joint sintering of electrodes at high temperature, Russ. J. Electrochem. 53 (2017) 873–879, https://doi.org/10.1134/S1023193517080043.

[63] I.N. Burmistrov, D.A. Agarkov, F.M. Tsybrov, S.I. Bredikhin, Preparation of membrane-electrode assemblies of solid oxide fuel cells by co-sintering of electrodes, Russ. J. Electrochem. 52 (2016) 669–677, https://doi.org/10.1134/S1023193516070053.

[64] I.N. Burmistrov, D.A. Agarkov, I.I. Tartakovskii, V.V. Kharton, S.I. Bredikhin, Performance optimization of cermet SOFC anodes: an evaluation of nanostructured Ni, ECS Trans. 68 (2015) 1265–1274 https://10.1149/06801.1265ecst.

[65] I. Burmistrov, D. Agarkov, S. Bredikhin, Y. Nepochatov, O. Tiunova, O. Zadorozhnaya, Multilayered electrolyte-supported SOFC based on NEVZ-ceramics membrane, ECS Trans. 57 (2013) 917–923 https://10.1149/05701.0917ecst.

[66] J.R. McBride, K.C. Hass, B.D. Poindexter, W.H. Weber, Raman and X-ray studies of Ce1-xRExO2-y, where RE = La, Pr, Nd, Eu, Gd and Tb, J. Appl. Phys. 76 (1994) 2435–2441, https://doi.org/10.1063/1.357593.

[67] G.M. Eliseeva, I.N. Burmistrov, D.A. Agarkov, A.A. Gamova, I.V. Ionov, A.A. Solovyev, I.I. Tartakovskii, S.I. Bredikhin, In-situ studies of processes at fuel electrode of solid oxide fuel cells (SOFC) by Raman spectroscopy, Chem. Prob. 3 (18) (2019) (accepted).

[68] G.M. Eliseeva, D.A. Agarkov, I.N. Burmistrov, A.A. Gamova, I.V. Ionov, S.I. Rabotkin, V.A. Semenov, A.A. Solovyev, I.I. Tartakovskii, S.I. Bredikhin, Raman spectra studies of inner “anode | electrolyte” interface on ESC and ASC SOFCs, ECS Trans. 91 (2019) (accepted).

[69] P. Briois, F. Lapostolle, V. Demange, E. Djurado, A. Billard, Structural investigations

of YSZ coatings prepared by DC magnetron sputtering, Surf. Coat. Technol. 201 (2007) 6012–6018, https://doi.org/10.1016/j.surfcoat.2006.11.016.
[70] Q. Xiao, H. Hongbo, S. Shao, J. Shao, Z. Fan, Influences of deposition rate and oxygen partial pressure on residual stress and microstructure of YSZ thin films, Thin Solid Films 517 (2009) 4295–4298, https://doi.org/10.1016/j.tsf.2008.11.138.
[71] S. Heiroth, R. Ghisleni, T. Lippert, J. Michler, A. Wokaun, Optical and mechanical properties of amorphous and crystalline yttria-stabilized zirconia thin films prepared by pulsed laser deposition, Acta Mater. 59 (2011) 2330–2340, https://doi.org/10.1016/j.actamat.2010.12.029.
[72] N. Mironova-Ulmane, A. Kuzmin, I. Steins, J. Grabis, I. Sildos, M. Pärs, Raman scattering in nanosized nickel oxide NiO, J. Phys. Conf. Ser. 93 (2007) 012039, , https://doi.org/10.1088/1742-6596/93/1/012039.